

RadarPLM: Adapting Pre-trained Language Models for Marine Radar Target Detection by Selective Fine-tuning

Qiyong Hu, Yaowen Li, Shengyi Zhang, Chuan Huang, Yu Liu, and You He

Abstract—Recent advances in pre-trained language models (PLMs) have demonstrated their capabilities in capturing universal knowledge, making them promising for radar signal processing applications. Nevertheless, directly fine-tuning PLMs on radar signals is both computationally expensive and prone to overfitting, particularly in low signal-to-clutter ratio (SCR) environments. In this paper, we propose a fine-tuning framework for PLM-based marine radar target detection. First, we design a lightweight adaptation module, enabling computationally efficient fine-tuning while preserving the pre-trained model’s general knowledge. Second, a novel preference-aware loss is developed to selectively optimize different feature patches based on their online-evaluated learning values, guiding the model to concentrate on those generalizable feature patterns during optimization. Finally, a binary classification head is retrained based on autoencoder network to further enhance detection performance. Experiments on real-world radar data show that the proposed RadarPLM framework yields at least a 6.35% improvement in detection performance over the existing networks under low SCR conditions. Especially, in the small-sample training cases, the proposed RadarPLM also achieves a significant advantage over existing networks owing to the incorporation of the PLM.

Index Terms—Marine small target detection, radar signal processing, pre-trained language models (PLMs), preference-aware loss.

I. INTRODUCTION

RADAR-based marine small target detection faces significant challenges due to the complex sea environment, especially under low signal-to-clutter ratio (SCR) conditions. Early research, exemplified by constant false alarm rate (CFAR) detectors, hinges on the precise modeling of statistical distributions to distinguish between targets and clutter. However, accurately characterizing the non-stationary and non-Gaussian distribution of sea clutter is inherently difficult, while distribution mismatches often result in excessive false alarm rates. Furthermore, as these traditional techniques typically exploit only a single amplitude feature, their detection performance is severely compromised in low SCR scenarios.

With the development of modern wide-band radars featuring high range and velocity resolution, approaches leveraging multi-domain features of radar echoes have gained significant attention. A series of hand-crafted features [1], [2], [3], [4], [5], including the phase, Doppler, and time-frequency domain

characteristics, have been devised for target detection. However, these methods rely heavily on hand-crafted heuristics and often fail to capture the nonlinear structures inherent in radar signal features.

Deep learning methods have been increasingly applied to small marine radar target detection, as they can directly and effectively learn discriminative nonlinear structures from radar signal features, offering a more flexible and powerful alternative to traditional hand-crafted approaches. Some studies use convolutional neural networks (CNNs) [6], [7], [8], [9], recurrent neural networks (RNNs) [10], and graph neural networks (GNNs) [11]. Among all the methods mentioned above, detectors based on sequence features and RNNs [10] or CNNs [9] offer an excellent trade-off between inference speed and detection performance.

Recently, the research community has experienced a paradigm shift from lightweight, task-specific neural networks toward large-scale foundation models. In particular, pre-trained large language models (LLMs), such as ChatGPT and DeepSeek, have demonstrated strong generalization capabilities across a wide range of complex tasks, including long-form text generation, mathematical reasoning, and code synthesis [12]. Motivated by these advances, an increasing body of research has extended these large models beyond the textual domain to non-textual data modalities, giving rise to multimodal large language models. Meanwhile, several recent studies [13], [14] have explored the adaptation of pre-trained large language models for time-series data analysis and wireless-communication signal processing. These works consistently report notable performance improvements over conventional lightweight task-specific models, particularly in scenarios characterized by limited labeled data. Inspired by these developments, this work investigates the feasibility and effectiveness of leveraging PLMs as a powerful backbone network for marine radar signal processing, aiming to enhance model robustness and generalization under challenging data conditions.

However, adapting PLMs to marine radar signal processing remains non-trivial, primarily due to two critical challenges: the need for parameter-efficient fine-tuning and the risk of model overfitting under complex real-world environments. First, the large parameter scale of PLMs necessitates lightweight and efficient fine-tuning strategies. Without such lightweight adaptation, the extensive computational and memory overhead of PLMs fine-tuning would limit their applicability in real-world radar scenarios. Lightweight adaptation

Qiyong Hu, Shengyi Zhang, Chuan Huang, Yu Liu, You He are with the Department of Electronic Engineering, Tsinghua University, Beijing 100084, China.

Yaowen Li is with the Shenzhen International Graduate School, Tsinghua University, Shenzhen 518055, China.

strategy requires reducing the number of trainable parameters by several orders of magnitude while preserving prior knowledge embedded in PLMs. Second, directly adapting PLMs to process radar signal features often leads to severe overfitting. This issue arises from the intrinsic characteristics of radar signal features. On the one hand, radar echoes typically suffer from low signal-to-noise ratios due to complex environmental noise and sensor limitations. Besides, in small marine target detection scenarios, weak target returns are frequently submerged by ocean clutter, producing mixed-status segments that bring noisy or anomalous patterns into the radar signal features. On the other hand, different feature patterns exhibit highly imbalanced convergence behaviors during fine-tuning: simple and regular patterns tend to converge rapidly, while more informative but complex patterns remain under-learned. Consequently, previous uniform optimization strategy may lead to severe overfitting, not only to noisy or anomalous patterns but also to overly simplistic ones. This highlights the necessity of a selective fine-tuning strategy that dynamically adjusts the training emphasis based on the learning value of each feature pattern.

To overcome the above issues, we develop a novel framework named RadarPLM (based on GPT2, an advanced open-source PLM). The proposed framework effectively bridges the gap between PLMs and radar target detection tasks with a lightweight adaptation module and a selective training strategy. First, we extract five sequence features from radar echo signals and patch them into multiple feature tokens. Subsequently, a radar target detector is built upon GPT2 and is fine-tuned through a lightweight adaptation module to efficiently align with the specific radar detection task. To mitigate overfitting, we design a preference-aware loss function, inspired by [15]. By introducing a selective training strategy to dynamically adjust the learning weights of different feature patches according to their online-evaluated learning values. Finally, the binary classification head is trained to further improve detection performance.

Our key contributions are summarized as follows:

- 1) We propose a novel framework RadarPLM based on GPT2 model, an advanced open-source PLM, for marine radar signal processing applications. To the best of our knowledge, this is the first work to demonstrate that the recent developed PLMs can serve as a strong starting point for model training and optimization on radar signal features.
- 2) For fine-tuning, we develop a lightweight adaptation module and design a novel selective training strategy, to reduce fine-tuning computational overhead and significantly mitigate the risk of model overfitting.
- 3) Extensive experiments validate that RadarPLM achieves state-of-the-art detection performance on popular marine radar datasets, especially in low SCR and small-sample training cases.

Our preliminary study [16] initially demonstrated the promising prospects of PLM for radar signal processing applications. In this paper, we further expand that work by introducing a lightweight adaptation module and selective

training strategy for more robust and generalizable optimization, achieving better performance.

The remainder of this paper is structured as follows. Section II briefly summarizes the related work. Section III presents the detailed operating procedure of the proposed RadarPLM. Section IV introduces the experimental results and analysis. Section V concludes our work.

II. RELATED WORK

A. Marine Radar Target Detection Based on Deep Learning

Deep learning models with elaborately crafted architectures have demonstrated great promise in marine target detection. Among them, Chen *et al.* [6] design a dual-channel CNN (DCCNN)-based structure detector that extracts both amplitude and time-frequency information from signals to achieve target detection. Qu *et al.* [7] introduce a CNN architecture augmented with asymmetric convolution layers to capture deep features of the time-frequency distribution. Xu *et al.* [8] propose a target detector in the case of limited training samples, utilizing pre-trained CNN to extract features from time-frequency spectrogram. Wan *et al.* [10] propose a sequence-based target detection framework that leverages instantaneous phase, Doppler spectrum, and short-time Fourier transform features, in conjunction with a bidirectional long-short-term memory (Bi-LSTM) network. Wang *et al.* [17] propose a target detector based on complex value U-Net (CV-UNet), which performs clutter suppression based on the amplitude-phase characteristics of radar echoes, and then achieves target detection. Su *et al.* [18] introduce a graph neural network (GNN) approach for radar target detection, which constructs spatio-temporal adjacency matrices, extracts hierarchical features through convolutional graph operations, and outputs detection results via nonlinear vertex embeddings.

In addition to traditional supervised learning, semi-supervised, unsupervised, and incremental learning approaches are proposed to further advance radar target detection. Wang *et al.* [19] propose a self-evolving framework for maritime radar target detection using semi-supervised learning, which enhances detection performance through unsupervised sample selection, data augmentation, and model optimization. Xia *et al.* [9] introduce an unsupervised contrastive learning framework that learns discriminative representations between targets and clutter from unlabeled data. Wang *et al.* [20] propose an incremental learning-based target detection method, which can continuously adapt the NN model in real time according to environmental changes. These methods provide compelling evidence that deep learning can significantly enhance detection performance without the need for explicit mathematical modeling. Despite their initial promise, these methods are inherently constrained by their dependence on relatively compact neural networks. Such models exhibit limited representational capacity, which hinders their ability to learn complex, high-dimensional feature representations. Consequently, they are particularly susceptible to performance degradation in the face of diverse and nonstationary environmental conditions. These challenges motivate us to first explore the use of PLMs for radar target detection.

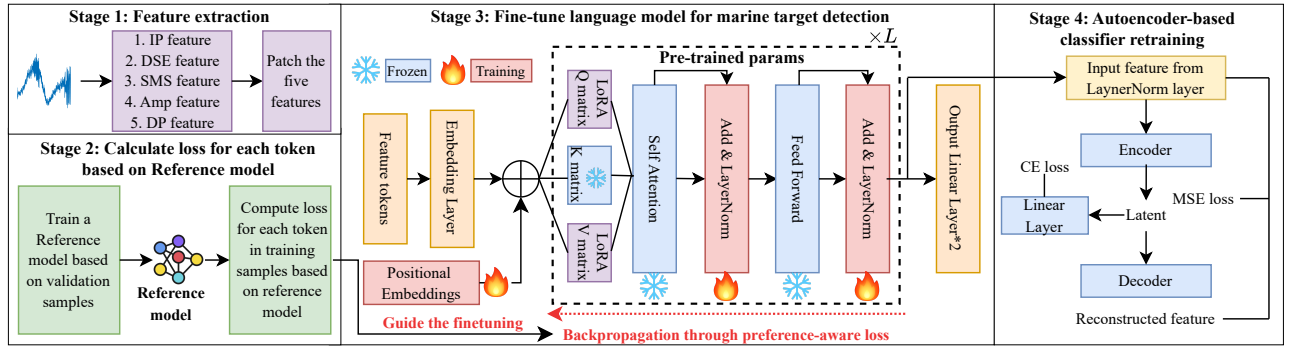


Fig. 1. Overview of our RadarPLM framework.

B. Signal Processing Based on Pre-trained Language Models

Recently, PLMs such as GPT2 and LLaMA2 have demonstrated exceptional capabilities in sequential signal processing and wireless communication tasks. For example, Zhou *et al.* [13] propose a unified time series analysis framework by fine-tuning frozen GPT2 [21] and achieving SOTA performance on various datasets. Liu *et al.* [22] propose a GPT2-empowered channel prediction framework to improve prediction accuracy. Sheng *et al.* [23] utilize the GPT2 model to develop an effective and robust beam prediction method. Zheng and Dai [24] propose a multi-task PLM framework to satisfy the requirements of different wireless communication tasks. IOT-LLM [25] directly utilize raw signal data as input and chain of thought prompts for reasoning on the Internet of Things (IOT) tasks.

However, none of these models are specifically devised for radar signal processing applications. In fact, recent studies [26] have raised significant concerns regarding the universal applicability and direct transferability of PLMs to various signal processing tasks. PLM-based approaches do not always deliver significant performance improvements, implying that their pre-trained parameters sometimes fail to transfer to downstream tasks. Especially, in marine radar target detection under low SCR conditions, directly fine-tuning a PLM often leads to severe overfitting issues, limiting its parameter transfer capability. To mitigate this limitation, we introduce a preference-aware loss that selectively trains on informative feature patches.

III. PROPOSED METHOD

A. Overview of the RadarPLM Framework

The overall framework of RadarPLM is illustrated in Fig. 1, which consists of four tightly connected stages: (1) sequence feature extraction and patching, (2) reference model training with token-level loss computation, (3) fine-tune LLMs for marine radar target detection, and (4) autoencoder-based binary classification head retraining.

To enable lightweight and generalizable fine-tuning of PLMs for radar target detection, the proposed RadarPLM framework integrates four tightly coupled modules into a

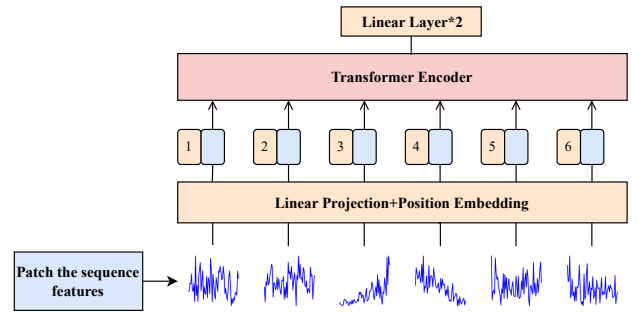


Fig. 2. Overview of the reference model.

unified optimization pipeline. First, the sequence feature extraction and patching module (Section III-B) derives five discriminative sequence features from the multi-domain transformation of radar echo signals. Then a patching module is devised to capture local semantic patterns while reducing computational complexity. Second, a lightweight adaptation module (Section III-C) is introduced to efficiently adapt the PLM backbone to the radar task, retaining its universal knowledge while minimizing parameter updates. Third, a preference-aware loss function (Section III-D), leveraging a lightweight reference model, enables selective optimization and mitigates overfitting. As shown in Fig. 1, the PLM-based model utilizes an input embedding layer to project feature patches into the PLM's encoder feature space. The embedded representations are processed by the initial encoder layers to extract more discriminative features. A layer normalization operation refines these features, producing the normalized representation F^{LN} , which enhances consistency and stability. Finally, two output linear layers generate token-level detection results. For the reference model structure, a standard Transformer encoder [27] processes the input feature patches to produce token-level detection outputs, as illustrated in Fig. 2. An autoencoder-based binary classification head (Section III-E) is retrained to further improve detection rate.

B. Sequence Feature Extraction and Patching

When the radar transmits coherent pulses toward the sea surface, it receives a sequence of echo signals from each

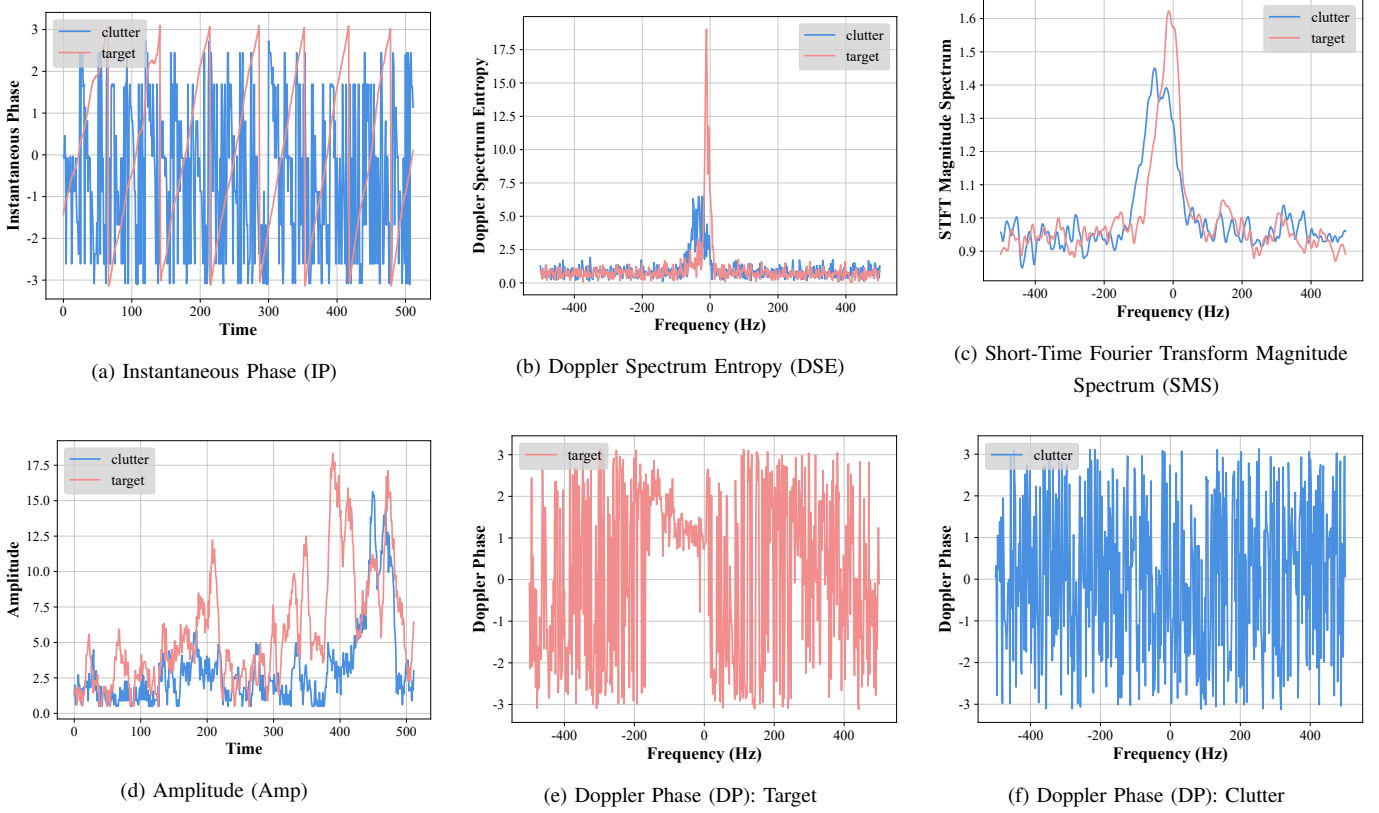


Fig. 3. IP, DSE, SMS, Amp, and DP features for target and sea clutter echo signal on IPIX dataset.

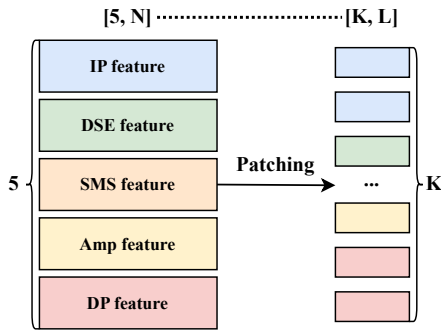


Fig. 4. An illustration of the patching operation.

range resolution cell. In clutter-dominated cells, these echoes primarily consist of sea surface backscatter and thermal noise, whereas in target-present cells, additional reflections from the target are superimposed. The received echo sequence x from a resolution unit can be decomposed into observation vectors x_i through the following segmentation:

$$x_i = [x(M \cdot (i - 1) + m)]_{m=1}^N, \quad i = 1, 2, \dots \quad (1)$$

where N represents the length of the observation window and M denotes the sliding step between consecutive observation vectors. Target detection is formulated as a binary hypothesis

testing problem:

$$\begin{cases} H_0 : \begin{cases} x(n) = c(n), & n = 1, 2, \dots, N \\ x_p(n) = c_p(n), & p = 1, 2, \dots, P \end{cases} \\ H_1 : \begin{cases} x(n) = s(n) + c(n), & n = 1, 2, \dots, N \\ x_p(n) = c_p(n), & p = 1, 2, \dots, P \end{cases} \end{cases} \quad (2)$$

where H_0 is the null hypothesis that indicates target absence in received signal $x(n)$, and H_1 is the alternative hypothesis that indicates target presence. In the cell under test, $s(n)$ and $c(n)$ denote target echos and sea clutter echos, respectively. Meanwhile, in the reference cells, $x_p(n)$ and $c_p(n)$ denote received echos and clutter echos, respectively. P is the number of reference cells. To effectively distinguish between the target echo and clutter echo, five unique sequence features are extracted from the time, phase, Doppler, and time frequency domains, as described below:

- Instantaneous Phase (IP): The instantaneous phase of the radar echo signal $x(n)$ is calculated as follow:

$$\phi(n) = \arg[x(n)], \quad (3)$$

where $\arg(\cdot)$ represents the phase of a complex variable.

- Doppler Spectrum Entropy (DSE): For the echo signal $x(n)$, its Doppler amplitude spectrum can be represented as:

$$F(f_d) = \frac{1}{\sqrt{N}} \left| \sum_{n=0}^{N-1} x(n) \exp(-j2\pi f_d n T_s) \right|, \quad (4)$$

where $f_d(-\frac{1}{2T_s} \leq f_d \leq \frac{1}{2T_s})$ represents the Doppler frequency, and T_s represents the pulse repetition interval

for the radar system. Furthermore, the entropy of the Doppler spectrum is calculated as:

$$\text{DSE}(F) = -\tilde{F}(f_d) \log \tilde{F}(f_d), \quad (5)$$

where $\tilde{F}(f_d) = \frac{F(f_d)}{\sum_{f_d} F(f_d)}$.

- **Short-Time Fourier Transform Magnitude Spectrum (SMS):** Due to the non-stationary characteristics of the radar echo signal, short-time fourier transform (STFT) provides a more comprehensive understanding compared to Doppler transform, which is calculated as:

$$S(k, m) = \sum_{n=-\infty}^{\infty} x(n)w(n-m)e^{-j2\pi\frac{kn}{\Omega}}, \quad (6)$$

where $w(\cdot)$ is the window function, Ω is the number of frequency bins, m represents the time index, and k is the frequency index. To make the features suitable for input into a sequence neural network, we compute the time-averaged magnitude of $S(k, m)$ and convert it into a decibel (dB) scale. Specifically, for each frequency index k , the following computation is performed:

$$\text{SMS}(k) = 10 \log_{10} \left(\sum_{m=0}^{N-1} |S(k, m)| \right). \quad (7)$$

- **Amplitude (Amp):** The instantaneous amplitude is computed by calculating the magnitude of the complex radar echo signal:

$$A(n) = |x(n)|. \quad (8)$$

- **Doppler Phase (DP):** The Doppler phase is extracted from the Doppler transform of echo signal:

$$\text{DP}(f_d) = \arg \left(\sum_{n=0}^{N-1} x(n) \exp(-j2\pi f_d n T_s) \right). \quad (9)$$

As illustrated in Fig. 3, the five extracted sequence features exhibit pronounced discriminability between target and clutter samples. To better structure the input for downstream processing, the extracted features are partitioned into non-overlapping patches. This patching approach offers several key advantages: it helps retain local semantic information, reduces the computational and memory burden of attention mechanisms. For a mini-batch of B samples, the input feature matrix is constructed by concatenating the IP feature F_{IP} , DSE feature F_{DSE} , SMS feature F_{SMS} , amplitude feature F_{Amp} , and DP features F_{DP} .

$$F = \text{Concat}(F_{\text{IP}}, F_{\text{DSE}}, F_{\text{SMS}}, F_{\text{Amp}}, F_{\text{DP}}). \quad (10)$$

Each feature in F is subsequently partitioned into non-overlapping patches of length L . If the final patch is shorter than L , zero padding is applied to ensure uniform length. The resulting K patches are concatenated to construct the final input tensor $F^{\text{P}} \in \mathbb{R}^{B \times K \times L}$, where $K = 5 \lceil \frac{N}{L} \rceil$. An illustration of this patching process is provided in Fig. 4.

C. Lightweight Fine-Tuning Module for the PLM Backbone

Adapting large-scale PLMs to specialized downstream applications like radar target detection presents significant challenges, necessitating a lightweight fine-tuning module. This necessity stems from two primary considerations. First, the immense parameter scale of PLMs renders full fine-tuning computationally expensive and often impractical for resource-constrained environments. Second, and more critically for radar target detection, available datasets are typically limited in size. Fine-tuning an entire model on such small datasets introduces the risks of catastrophic forgetting, where the model's valuable pre-trained knowledge is overwritten, and overfitting, due to data scarcity.

Drawing inspiration from recent work [13], [28], we propose a lightweight fine-tuning module designed to balance this trade-off between adaptability and efficiency. Our approach is guided by two hypotheses, consistent with [13], [28]: (1) achieving strong performance does not require updating all network parameters; instead, updating a small subset, such as bias terms or specific layers, while keeping the majority frozen is sufficient. (2) The weight updates during adaptation possess a low "intrinsic rank." Consequently, instead of modifying the entire weight matrix, we can capture task-specific knowledge within a much smaller, low-rank subspace. Our module implements these insights by jointly updating the layer normalization parameters and incorporating a Low-Rank Adaptation (LoRA) component.

Concretely, we apply LoRA to the query and value projection matrices, \mathbf{W}_Q and \mathbf{W}_V , within each attention block of the PLM backbone, as illustrated in Fig. 5. For a given frozen weight matrix \mathbf{W} , LoRA introduces two low-rank trainable matrices, A and B , and modifies the transformation as follows:

$$\mathbf{W} \leftarrow \mathbf{W} + AB^T, \quad (11)$$

where $\mathbf{W} \in \mathbb{R}^{d_1 \times d_2}$, $A \in \mathbb{R}^{d_1 \times r}$, $B \in \mathbb{R}^{d_2 \times r}$, and $r \ll \min(d_1, d_2)$. The low-rank decomposition effectively projects the task-specific adaptation into a compact subspace, greatly reducing the parameter footprint while retaining original pre-trained knowledge. The matrices are initialized as $A \sim \mathcal{N}(0, \sigma^2)$ and $B = 0$, ensuring stable convergence and preventing interference with pre-trained weights during the early training phase. During fine-tuning, only A and B are updated, while \mathbf{W} remains fixed. Owing to the low-rank constraint: $r \ll \min(d_1, d_2)$, the number of parameters for fine-tuning A and B , i.e., $rd_1 + rd_2$, is significantly less than that of the full weight matrix, $d_1 d_2$. The reduced parameter size thus makes the fine-tuning much efficient.

This design offers two key advantages. First, this module mitigates the computationally expensive limitation of full fine-tuning by updating only a very small subset of the network parameters and compact low-rank matrices, thereby reducing trainable parameters by several orders of magnitude. Second, this module alleviates catastrophic forgetting of pre-trained knowledge during adaptation, as the newly acquired information is encoded within a subspace rather than the original representation. Consequently, this module enables the finetuned model to retain its pre-trained general-purpose

knowledge while efficiently adapting to downstream radar tasks.

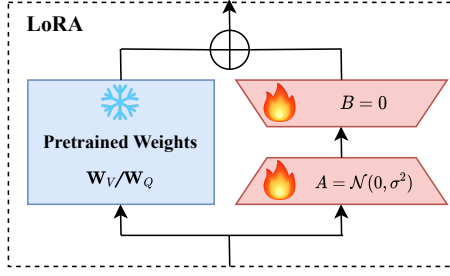


Fig. 5. Illustration of the LoRA fine-tuning process.

D. Preference-Aware Loss Function

1) *Methodology*: To address the prevalent issue of overfitting in PLM-based model fine-tuning, we introduce a preference-aware loss function to enable selective training, a novel strategy designed to guide the model towards learning generalizable feature patterns. During fine-tuning, feature patches dominated by clutter-induced noise or anomalies can mislead the model and hinder effective learning. Conventional optimization methods, which treat all feature patterns indiscriminately with a standard cross-entropy loss, are prone to memorizing these non-generalizable, instance-specific characteristics, leading to severe overfitting.

In contrast, our proposed selective training strategy follows a "preference-aware" philosophy. The core idea is to evaluate the learning value of each feature patch during training and use this evaluation to reweight its contribution to the final loss. This approach enables the model to focus on feature patterns with high learning values while minimizing the impact of noisy or anomalous patterns. By preventing the model from overfitting to these non-generalizable patterns, this strategy enhances model robustness and mitigates overfitting.

Specifically, for each feature token $F_{b,k}^{\text{fi}}$ within a training batch, we compute two distinct loss values:

- **Reference Loss** $\mathcal{L}_{\theta_r, b, k}(F_{b,k}^{\text{fi}})$: This loss is computed using a lightweight reference model θ_r , which has been trained on the validation set. It serves as a stable proxy for evaluating the feature patch's inherent difficulty or noise level:

$$\mathcal{L}_{\theta_r, b, k}(F_{b,k}^{\text{fi}}) = - \sum_i y_{b,k}^i \log(\hat{y}_{b,k}^{i, \theta_r}), \quad (12)$$

where $\hat{y}_{b,k}^{i, \theta_r}$ is the prediction from lightweight reference model θ_r .

- **Target Loss** $\mathcal{L}_{\theta_t, b, k}(F_{b,k}^{\text{fi}})$: his loss is calculated using the predictions from the current PLM-based model θ_t being fine-tuned, which reflects how well the model currently fits the feature patch:

$$\mathcal{L}_{\theta_t, b, k}(F_{b,k}^{\text{fi}}) = - \sum_i y_{b,k}^i \log(\hat{y}_{b,k}^{i, \theta_t}), \quad (13)$$

where $\hat{y}_{b,k}^{i, \theta_t}$ represents the prediction from the current PLM-based model θ_t .

The key to our method is computing an evaluated learning value $s_{b,k}$ based on the discrepancy between the target and reference losses:

$$s_{b,k} = \text{ReLU}(\mathcal{L}_{\theta_t, b, k}(F_{b,k}^{\text{fi}}) - \alpha \mathcal{L}_{\theta_r, b, k}(F_{b,k}^{\text{fi}})), \quad (14)$$

where α is a scaling coefficient, and the $\text{ReLU}(\cdot)$ function, defined as $\text{ReLU}(x) = \max(0, x)$, ensures that only tokens with positive excess loss are fine-tuned.

This loss difference naturally leads to a selective training scheme with desirable properties:

- **High Importance (Unlearned)**: If \mathcal{L}_{θ_t} is much larger than $\alpha \mathcal{L}_{\theta_r}$, the feature token is identified as containing valuable, yet unlearned patterns.
- **Low Importance (Noisy/Anomalous patterns)**: If $\alpha \mathcal{L}_{\theta_r}$ is large (indicating feature token with inherent noisy/anomalous patterns), it effectively dampens $s_{b,k}$, even if \mathcal{L}_{θ_t} is large, preventing model overfitting.
- **Low Importance (Well Learned)**: If \mathcal{L}_{θ_t} is already small, the feature token is considered well learned, and $s_{b,k}$ will also be small, preventing redundant updates to easy patterns.

The final training loss is a weighted sum over all feature tokens across the mini-batch, where each token's contribution is scaled by a token-level importance score:

$$\mathcal{L}_{\text{final}} = \frac{1}{B * K} \sum_{b=1}^B \sum_{k=1}^K s_{b,k} \cdot \mathcal{L}_{\theta_t, b, k}(F_{b,k}^{\text{fi}}). \quad (15)$$

where B and K denote the batch size and the number of feature tokens, respectively.

2) *Theoretical Insight of the Effectiveness of Feature Token Importance*:

A. Problem Definition: Inspired by [15], we begin by formalizing an optimization problem of selecting useful feature patches for model fine-tuning. At each training step t , given a candidate set B_t , the objective is to select a feature patch $(F_{b,k}^{\text{fi}}, y_b^k) \in B_t$ whose inclusion in the training set D_t maximally reduces the generalization loss on the unseen holdout set D_{ho} . This can be expressed as the following optimization problem:

$$\arg \min_{(F_{b,k}^{\text{fi}}, y_b^k) \in B_t} - \log p(y^{\text{ho}} | F^{\text{ho}}; D_t \cup (F_{b,k}^{\text{fi}}, y_b^k)). \quad (16)$$

However, directly optimizing (16) is computationally prohibitive, as it requires retraining the model for each candidate patch. To enable a practical surrogate, we reformulate this objective using probabilistic decomposition.

B. Derivation of the Surrogate Objective: Applying Bayes' theorem, the term in (16) can be decomposed as:

$$\begin{aligned} & - \log p(y^{\text{ho}} | F^{\text{ho}}; D_t \cup (F_{b,k}^{\text{fi}}, y_b^k)) \\ & = - \log \frac{p(y, y^{\text{ho}} | F, F^{\text{ho}}, D_t)}{p(y | F; D_t)}. \end{aligned} \quad (17)$$

Assuming that each label is statistically independent of all other labels in the corpus when conditioned on its corresponding feature vector, the joint probability term in the numerator can be expressed as follows:

$$\begin{aligned} p(y, y^{\text{ho}} | F, F^{\text{ho}}, D_t) &= p(y | F; F^{\text{ho}}, y^{\text{ho}}, D_t) p(y^{\text{ho}} | F^{\text{ho}}; F, D_t) \\ &= p(y | F; y^{\text{ho}}, F^{\text{ho}}, D_t) p(y^{\text{ho}} | F^{\text{ho}}; D_t). \end{aligned} \quad (18)$$

Substituting (18) into (17) and taking the logarithm yields:

$$\begin{aligned} &\log p(y^{\text{ho}} | F^{\text{ho}}; D_t \cup (F_{b,k}^{\text{fi}}, y_b^k)) \\ &= \log \frac{p(y | F; y^{\text{ho}}, F^{\text{ho}}, D_t) p(y^{\text{ho}} | F^{\text{ho}}, D_t)}{p(y | F; D_t)} \quad (19) \\ &\propto \log p(y | F; y^{\text{ho}}, F^{\text{ho}}, D_t) - \log p(y | F; D_t) \\ &\propto \mathcal{L}[y_b^k | F_{b,k}^{\text{fi}}; D_t] - \mathcal{L}[y_b^k | F_{b,k}^{\text{fi}}; D_t, D_{\text{ho}}]. \end{aligned}$$

In summary, for a model trained on D_t , the process of identifying the feature patch that minimizes the loss on the holdout samples in (16) can be approximated by the following objective:

$$\arg \max_{(F_{b,k}^{\text{fi}}, y_b^k) \in B_t} \mathcal{L}[y_b^k | F_{b,k}^{\text{fi}}; D_t] - \mathcal{L}[y_b^k | F_{b,k}^{\text{fi}}; D_t, D_{\text{ho}}]. \quad (20)$$

Here, $\mathcal{L}[y_b^k | F_{b,k}^{\text{fi}}; D_t]$ denotes the training loss on the patch using the current model trained on D_t , whereas $\mathcal{L}[y_b^k | F_{b,k}^{\text{fi}}; D_t, D_{\text{ho}}]$ represents the expected irreducible holdout loss obtained if the model were trained on both the training set and the unseen holdout set. This objective reveals that the difference between the training loss and the irreducible holdout loss effectively quantifies the reducible component of the generalization error contributed by each feature patch. Consequently, this loss discrepancy can be rigorously interpreted as the learning value of the patch, representing the marginal improvement in performance on unseen data expected from its inclusion in the training process.

C. Practical Implementation and Approximation: However, realizing the irreducible loss in practice for deep neural networks presents several significant challenges. We introduce the following strategic approximations to enable an efficient and tractable implementation for calculating the irreducible loss inspired by [15]:

- 1) The theoretical derivation relies on Bayesian inference and conditioning. As exact Bayesian inference is intractable in neural network, we fit the model using Stochastic Gradient Descent (SGD) instead.
- 2) In addition, we adopt the validation set (D_{val}) as the holdout set to serve as a statistically sound proxy for the unseen data distribution.
- 3) Furthermore, since training the PLM-based model on the combined set $D_t \cup D_{\text{val}}$ is computationally expensive, we approximate it using the loss computed by a lightweight transformer-based model (reference model) trained on D_{val} .

D. Conclusion: The calculated gap between the target loss $\mathcal{L}_{\theta_t, b, k}(F_{b,k}^{\text{fi}})$ and the approximated irreducible loss $\mathcal{L}_{\theta_r, b, k}(F_{b,k}^{\text{fi}})$ (derived from the lightweight reference model)

serves as a practical measure of each feature patch's learning value, which forms the token weights in (14). Accordingly, the loss gap is employed to adaptively reweight the training objective, guiding the model to focus on learning informative and unlearned feature tokens, while significantly reducing the impact of noisy and trivial patterns.

3) Comparison with Existing Loss Designs:

Most existing loss improvements for marine radar target detection address issues such as sample imbalance, hard sample learning, or false alarm control. Various solutions have been proposed, including enhanced focal loss that emphasizes learning from hard or moderately difficult samples [29], and Neyman-Pearson criterion-inspired loss that effectively regulates the false alarm rate [30]. However, these approaches seldom address a crucial issue: mitigating model overfitting in complex real-world scenarios, particularly under low SCR conditions. In contrast, the proposed preference-aware loss incorporates a selective training mechanism that directs the model's attention to transferable and informative patterns, thus substantially reducing the risk of overfitting. Moreover, while sample reweighting strategies are often employed to alleviate overfitting by defining a weighting function that maps the training loss to a corresponding sample weight, our method adopts a patch-level reweighting strategy motivated by the uneven distribution of informative patterns across multi-domain radar features. This design enables a more fine-grained and flexible learning process. In general, the proposed preference-aware loss marks a major and substantial advance in enhancing model generalization across diverse and low-SCR radar detection scenarios.

E. Autoencoder-Based Binary Classification Head Retraining

As shown in Fig. 1 and Section III-A, the PLM-based network produces token-level outputs of shape $[B, K, 2]$, which is inconvenient for final decision. To obtain a binary output for each sample, we therefore retrain an autoencoder-based binary classification head on top of high-dimensional feature representation F^{LN} . It comprises: (1) an encoder with convolutional and fully connected layers producing compact discriminative representation; (2) a symmetric decoder ensuring feature consistency through reconstruction; and (3) a classification head operating on the latent vector. The autoencoder is optimized by a dual-objective loss combining reconstruction and classification terms:

$$\mathcal{L}_{\text{recon}} = \left\| F^{\text{LN}} - \hat{F}^{\text{LN}} \right\|_2^2. \quad (21)$$

$$\mathcal{L}_{\text{ce}} = -\frac{1}{B} \sum_{b=1}^B \sum_{i=1}^2 y_b^i \log \hat{y}_b^i. \quad (22)$$

A task-uncertainty weighting scheme [31] adaptively balances these objectives:

$$\mathcal{L}_{\text{total}} = \frac{1}{2\sigma_{\text{recon}}^2} \mathcal{L}_{\text{recon}} + \frac{1}{\sigma_{\text{ce}}^2} \mathcal{L}_{\text{ce}} + \log \sigma_{\text{recon}} \sigma_{\text{ce}}, \quad (23)$$

where σ_{recon} and σ_{ce} are learnable task uncertainties that regulate the joint optimization dynamics.

Algorithm 1 RadarPLM Training Protocol**Require:**

Radar echo signals $\{x(n)\}_{n=1}^N$ and Target labels $\{y_b\}_{b=1}^B$
 PLM parameters θ_{PLM}

1: Stage 1: Sequence Feature Extraction

- 1) Extract IP, DSE, SMS, Amp, and DP features from the observation vector, respectively, see (3), (4), (5),(7), and (9).
- 2) Patch the five features into feature tokens, see Fig. 4.

2: Stage 2: Reference Model Training

- 1) Train a lightweight reference model θ_r based on validation samples and CE loss.
- 2) Compute the loss for each feature token of the training samples based on the predicted output probabilities of θ_r , see (12).

3: Stage 3: Fine-tune PLM for Target Detection

- 1) Compute the loss for each feature token of the training samples based on the predicted output probabilities of current model, see (13).
- 2) Fine-tune PLM for target detection via lightweight adaptation module and preference-aware loss function, see (14) and (15).

4: Stage 4: Binary Classification Head Retraining

- 1) Train autoencoder-based binary classification head based on the weighted sum of reconstruction loss and CE loss, see (21), (22), and (23).
- 2) Adjust detection threshold η for controllable FAR, see (24).

Ensure:

Fine-tuned RadarPLM model with controllable FAR.

During inference, false alarm rate is controlled via threshold-setting using sorted softmax outputs of clutter samples. The detection threshold η is then determined based on the desired false alarm rate P_{fa}^d as follows:

$$\eta = O_{\text{sorted}}(x), \quad x = \lceil P_{fa}^d \times N_{\text{clutter}} \rceil, \quad (24)$$

where $O_{\text{sorted}}(x)$ is the x -th largest output and N_{clutter} is the total number of test clutter samples. The overall procedure of the RadarPLM is presented in Algorithm 1.

IV. EXPERIMENTS

In this section, we first describe the experimental setup, followed by a comprehensive evaluation of RadarPLM's detection performance under two settings: sufficient training data and limited training data scenarios.

A. Experimental Setup

1) *Dataset*: We employ eight benchmark data sequences (Data1–Data8) from the Intelligent Pixel Processing X-band (IPIX) radar archive, summarized in Table I. All datasets were recorded in 1993 by the IPIX radar on the east coast of Canada and include full polarization measurements (HH, HV, VH, and VV). Each set contains 14 range cells sampled at 1 kHz, with 131 072 complex echoes per cell, yielding an

observation window of 0.512 s per sample. Returns from the primary range cell constitute target echoes, whereas returns from the remaining clutter-only cells represent sea clutter. To facilitate performance analysis in varying operating conditions, Data1–Data3 correspond to low signal-to-clutter ratio (SCR) scenes, while Data4–Data8 represent high-SCR scenes.

To ensure sufficient training data, we employ overlapped segmentation following the partition rule in (1), with parameters set to $M = 32$ for target cells and $M = 128$ for clutter cells. This process generates 4,079 target samples and more than 9,000 clutter samples per dataset. The samples are divided into three groups: (1) a training set using the first 20% observation time for both the target and clutter cells, (2) a validation set covering 20% to 35% of the observation time, and (3) a test set containing the remaining samples.

2) *Baselines*: To validate the superiority of RadarPLM, eight deep learning-based marine radar target detection methods are implemented as baselines. Among them, RNN, Bi-LSTM, GRU, Transformer, PatchTST, and ResNet18 represent lightweight models that process sequence features; OFA uses a PLM backbone to process sequence features; and ADN18 utilizes time-frequency maps and enhanced CNNs for detection.

- RNN [10]: RNN is a sequential neural architecture with temporal feedback loops. In experiments, the number of RNN layers and the hidden layer nodes are set to 2 and 6, respectively.
- Bi-LSTM [10]: Bi-LSTM enhances traditional long-short-term memory (LSTM) by incorporating bidirectional processing. In our implementation, the number of LSTM layers and the number of hidden units per layer are set to 2 and 6, respectively.
- GRU [32]: GRU employs simplified gating mechanisms compared to LSTM. In experiments, the number of GRU layers and the hidden layer nodes are set to 2 and 8, respectively.
- Transformer [27]: Transformer reshapes sequence processing through self-attention mechanisms. In experiments, the Transformer encoder is configured with a model dimensionality of 32, comprising 2 layers and 8 attention heads. The feed-forward network (FFN) within each layer is designed with a hidden size of 128.
- PatchTST [33]: PatchTST segments the sequence features into local patches and leverages a Transformer encoder to model them. In experiments, the Transformer encoder is configured with a model dimensionality of 64, comprising 2 layers and 16 attention heads. The feed-forward network (FFN) within each layer is designed with a hidden size of 128.
- ResNet18 [9]: ResNet18 is a convolutional architecture adapted for analyzing time series by modifying input channels, leveraging residual blocks to capture temporal patterns.
- OFA [13]: OFA patches input sequence features, feeds them through a frozen GPT2 model with trainable positional embeddings and LayerNorm, and uses a final linear layer for classification.
- ADN18 [34]: ADN18 enhances CNN model with asym-

TABLE I
OVERVIEW OF THE IPIX DATABASE.

Label	Name	File Name	Target Distance Bin	SCR
1	17	19931107_135603_starea	9	Low
2	25	19931108_213827_starea	7	Low
3	26	19931108_220902_starea	7	Low
4	54	19931111_163625_starea	8	High
5	280	19931118_023604_stareC0000	8	High
6	283	19931118_035737_stareC0000	10	High
7	311	19931118_162658_stareC0000	7	High
8	320	19931118_174259_stareC0000	7	High

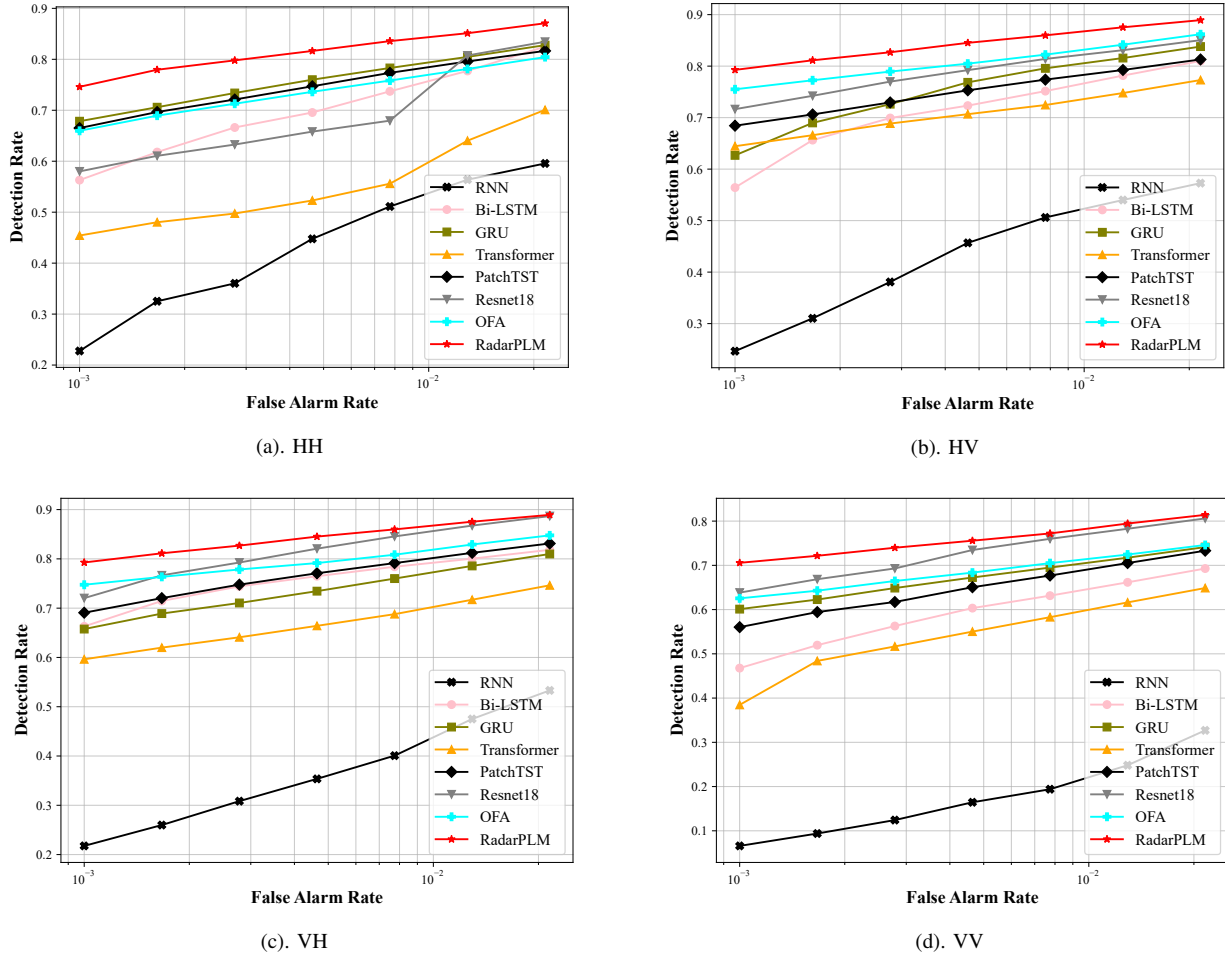


Fig. 6. Comparison of model detection performance on various datasets. The accompanying ROC curves demonstrate that the RadarPLM framework achieves the best overall detection performance.

TABLE II
HYPERPARAMETERS FOR NETWORK TRAINING.

Parameter	Value
Batch size	64
Eval batch size	400
Epochs for RadarPLM fine-tuning	500
Epochs for Autoencoder training	300
Optimizer	Adam (betas=(0.9,0.999))
Learning rate for PLM fine-tuning	0.0001
Learning rate for Autoencoder training	0.00001

metric convolutional kernels and attention mechanism to adaptively capture spatial-temporal features in spectro-

grams derived from Short-Time Fourier Transform.

3) *Evaluation Metrics:* In maritime target detection, achieving a high detection rate at an extremely low false alarm rate is imperative, as misinterpreting sea clutter as targets can have significant consequences, particularly in military operations. We evaluated the detection performance of different detectors at a false alarm rate of 0.005, considering that our test set only comprises 6,000 clutter samples. Selecting a lower false alarm rate could result in unstable comparisons due to the limited number of clutter samples.

4) *Implementation Details:* The experimentally relevant hyperparameters and details are shown in Table II. For patching, the size of feature patches is set to 48. For the PLM, the

TABLE III
COMPARISON OF DETECTION RATES (%) ON SUFFICIENT TRAINING SAMPLES UNDER DIFFERENT SIGNAL-TO-CLUTTER RATIO (SCR) CONDITIONS.

Method	All Data					Low SCR Data				
	HH	HV	VH	VV	AVG	HH	HV	VH	VV	AVG
RNN [10]	46.04	46.66	38.18	17.04	36.98	9.45	13.00	11.67	4.47	9.65
Bi-LSTM [10]	70.39	73.15	76.48	60.89	72.48	39.38	42.47	37.48	25.27	36.15
GRU [32]	76.46	77.55	73.96	67.48	73.86	48.99	50.46	49.79	27.33	44.14
Transformer [27]	52.95	71.73	67.32	55.67	61.92	32.31	41.89	46.43	15.35	34.00
PatchTST [33]	75.23	75.72	77.49	66.59	73.76	49.27	49.71	53.18	31.46	45.91
ResNet18 [9]	66.24	80.96	82.31	73.97	75.87	50.45	56.18	53.73	44.54	51.23
OFA [13]	74.19	80.38	79.71	70.36	76.16	49.28	54.18	54.62	26.96	46.26
ADN18 [34]	79.74	83.50	82.01	78.02	80.82	54.76	60.04	31.32	46.11	47.31
RadarPLM	82.51	84.81	84.61	75.90	81.96	60.03	63.19	62.27	44.82	57.58

Note: All results are evaluated at a false alarm rate (P_{fa}) of 0.005. The best and second-best results are highlighted in red and blue, respectively.

smallest version of GPT2 with $F = 768$ feature dimension and the first $L = 4$ layers of the GPT2 encoder are deployed. The value of α in (14) is set to 0.9. All signal feature extraction operations are performed with MATLAB R2016a software. All network training experiments are conducted on a system equipped with an E5-2695v3 CPU, an NVIDIA 3090Ti GPU, and 64 GB of RAM.

B. Average Performance Comparison

Table III reports the detection rates achieved by RadarPLM and the eight baseline detectors introduced in Section IV-A2. All results are obtained with a fixed false alarm rate of 0.005 on the eight IPIX datasets. Compared to the best competing sequence feature detector, RadarPLM improves the detection rate by 7.60%, 3.85%, 2.30%, and 1.93% for the HH, HV, VH, and VV polarizations, respectively. Fig. 6 presents the complete ROC curves; it is evident that RadarPLM maintains the highest detection probability across the full range of false alarm rates. We also compare RadarPLM with ADN18, which relies on high-dimensional time–frequency maps and an enhanced CNN backbone. Despite using only compact sequence features, RadarPLM still delivers a 1.14% gain in the average detection rate.

Furthermore, we compare RadarPLM with other baseline models in terms of training complexity, total network parameters, and inference cost to evaluate its practicality for real-world deployment. The comparison results are summarized in Table IV. Although RadarPLM has the highest total network parameters, the number of trainable parameters is comparable to those of other models, as the majority of its weights are frozen during fine-tuning. In particular, RadarPLM achieves an exceptionally low average inference latency. Specifically, it requires only 5.6561 seconds to process more than 9,000 test samples, which is 28.44 times faster than the ADN18 method. This efficiency is primarily attributed to our patching strategy, which substantially reduces the number of feature tokens, and consequently, the computational overhead. Moreover, the intrinsic inference acceleration of the GPT architecture further enhances this performance gain. Together, these advantages

make RadarPLM a promising solution for real-time marine target detection.

C. Performance Comparison on Low SCR Data

Owing to the inherent complexity of the marine environment, low-SCR radar echoes are frequently encountered in practical applications. In such scenarios, clutter-induced noise gives rise to noisy and anomalous feature patterns, leading to pronounced performance degradation in existing detection algorithms. To assess model robustness, we evaluate each approach on more challenging low-SCR datasets (IPIX #17, IPIX #25, and IPIX #26), where the SCR typically falls below 5 dB.

As shown in the right section of Table III, while most baselines suffer from severe performance degradation due to strong clutter-induced noise, RadarPLM maintains a remarkable lead. It achieves an average detection rate of 57.58% on low SCR datasets, surpassing the second-best method (ResNet18) by 6.35% and the complex ADN18 method by a significant margin of 10.27%. This result highlights the critical advantage of our method in learning discriminative representation from noisy and anomalous radar signal features.

D. Small-sample Training Condition

Due to the inherent sparsity of radar targets in real-world scenarios, obtaining high-quality labeled samples for radar target detection presents a substantial challenge. Considering this issue, we conducted experiments under scarce training sample conditions to assess the effectiveness of RadarPLM. Specifically, we utilized a data split ratio of 10% (Training samples): 5% (Validation samples): 85% (Test samples), where the number of training samples are severely reduced.

In Fig. 7, we present a comparative analysis of all methods under the scarce training sample condition against the standard setting (Abundant Training Samples) described in Section IV-B. The results clearly demonstrate that RadarPLM exhibits the second-lowest performance degradation among all assessed methods, highlighting its robustness to scarce

TABLE IV
NETWORK PARAMETERS (TRAINING PARAMETERS / TOTAL PARAMETERS) AND AVERAGE INFERENCE TIME OF DIFFERENT METHODS.

Detector	Avg. inference time (s)	Total Params (M)	Trainable Params (M)
RNN [10]	5.3587	0.0003	0.0003
Bi-LSTM [10]	5.6028	0.0016	0.0016
GRU [32]	5.7746	0.0008	0.0008
Transformer [27]	6.0678	0.0611	0.0611
PatchTST [33]	5.3727	0.0939	0.0939
ResNet18 [9]	5.4434	3.8454	3.8454
ADN18 [34]	160.9018	14.3315	14.3315
RadarPLM	5.6561	69.3932	2.4567

data availability. Specifically, RadarPLM achieves a substantial increase of **19.66%** in the average detection rate over the previously proposed sequence-feature based detector [10]. This marked improvement can be mainly attributed to three key factors:

- First, The embedded knowledge from pre-trained parameters endows RadarPLM with a highly advantageous parameter initialization. This acts as a powerful springboard for optimization, enabling effective convergence even in data-limited regimes and drastically mitigating the data-hungry nature of conventional training paradigms.
- Second, the substantial parameter scale of RadarPLM inherently grants robustness to distributional variations, enabling superior generalization compared to smaller-scale neural networks. Its extensive capacity allows it to capture complex data structures and efficiently handle variability in different radar detection scenarios.
- Third, the integration of a preference-aware loss function significantly improves RadarPLM detection performance, especially in challenging scenarios characterized by low SCR.

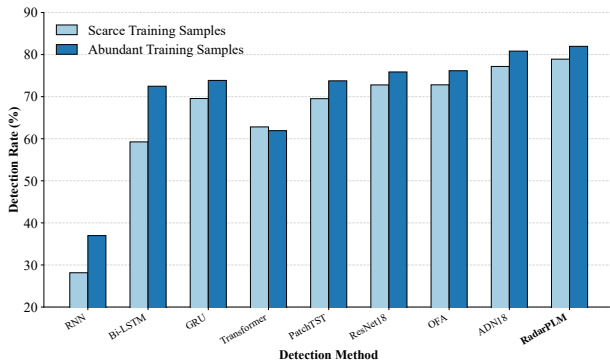


Fig. 7. Performance comparison under small and abundant sample training conditions. The result shows that the RadarPLM approach experiences substantially smaller performance degradation under scarce training sample condition while maintaining the best overall detection performance.

E. Ablation Study

1) *Backbone Architectures*: To validate the effectiveness of the backbone choice, the ablation study is conducted in this section by removing or replacing the PLM under sufficient training samples setting:

- 1) RadarPLM (0): In this variant, the PLM backbone is entirely removed, while all other components of the framework are kept unchanged.
- 2) RadarPLM (T): In this variant, the PLM backbone is replaced with a randomly initialized transformer block.
- 3) RadarPLM (R): In this variant, the network architecture and fine-tuning procedure are maintained, but pre-trained parameters of PLM are replaced with random initialization.

In Table VI, we show the results of the ablation study on backbone choice. It can be seen that the removal or exchange of PLM backbone results in notable performance degradation, indicating the necessity of PLM for high detection performance.

2) *Fine-tuning Strategies*: To verify the effectiveness of the proposed fine-tuning strategy, we conducted an ablation study under the setting of sufficient training samples, as summarized in Table V, and the corresponding results are presented in Table VI. In this experiment, four fine-tuning configurations were evaluated: (1) RadarPLM: jointly fine-tuning the LoRA modules and Layer Normalization (LN) parameters, (2) RadarPLM (LoRA): fine-tuning only the LoRA modules, (3) RadarPLM (LN): fine-tuning only the LN parameters, and (4) RadarPLM (F): full fine-tuning of all model parameters. As shown in the results, the joint fine-tuning of LoRA and LN achieves notably higher performance, while maintaining a relatively shorter training cost (0.116 h/100 epochs) than full fine-tuning (0.148 h/100 epochs). This demonstrates that the proposed design not only enhances model adaptability, but also significantly reduces computational cost.

3) *Loss Function*: In addition, we compare the fine-tuning effects of preference-aware loss and CE loss on low SCR datasets. First, to facilitate a direct and quantitative comparison between the two loss functions, we aggregated the outputs of all feature tokens by applying a softmax normalization function followed by averaging operation. The resulting probabilities are then used for target detection. In Fig. 8, we present the detection rates on test samples from different low-SCR datasets under HH polarization across multiple training epochs. It can be observed that preference-aware loss achieves an improvement of around **1%-12%** compared to cross-entropy loss (uniformly optimized on all feature patches) in different training epochs and datasets. We also include the performance of the reference model (gray line) for comparison. it can be seen that the optimal detection performance of

TABLE V
ABLATION STUDY ON FINE-TUNING STRATEGY CONFIGURATIONS AND THEIR CORRESPONDING TRAINING TIME (MEASURED OVER 100 TRAINING EPOCHS).

Model	LoRA	Layer Norm	Other Params	Training Time (hour/100 epochs)
RadarPLM	✓	✓		0.116
RadarPLM (F)		✓	✓	0.148
RadarPLM (LoRA)	✓			0.116
RadarPLM (LN)		✓		0.112

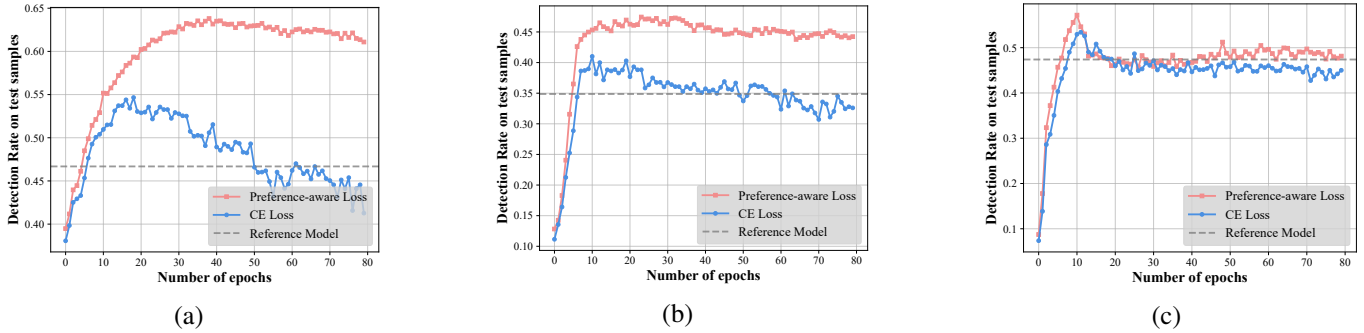


Fig. 8. Comparison of detection rates achieved by the proposed preference-aware loss and the conventional cross-entropy (CE) loss under HH polarization across different datasets ((a) IPIX #17, (b) IPIX #25, and (c) IPIX #26) over training epochs. The results demonstrate that while the CE loss exhibits detection rate degradation shortly after a few training epochs (indicating overfitting), the preference-aware loss effectively mitigates overfitting, enabling consistent performance improvement throughout more training epochs.

TABLE VI
RESULTS OF ABLATION STUDY ON THE BACKBONE CHOICE AND FINE-TUNING STRATEGIES.

Model	HH	HV	VH	VV	AVG
RadarPLM	82.51	84.81	84.61	75.90	81.96
Backbone Choice Ablation					
RadarPLM (O)	77.51	79.38	80.35	69.97	76.80
RadarPLM (T)	78.25	79.77	81.16	72.13	77.83
RadarPLM (R)	75.19	75.44	75.81	65.15	72.90
Fine-tuning Strategy Ablation					
RadarPLM (F)	81.69	83.45	84.41	74.07	80.91
RadarPLM (LoRA)	82.20	84.45	84.56	75.53	81.69
RadarPLM (LN)	82.33	83.73	83.80	75.12	81.25

Note: RadarPLM(O)–RadarPLM(R) denote backbone ablation results, while RadarPLM(F)–RadarPLM(LN) denote fine-tuning strategy ablation results. The best and second-best results are highlighted in **red** and **blue**, respectively.

TABLE VII
RESULTS OF ABLATION STUDY ON THE LOSS FUNCTION.

Method	Data1	Data2	Data3	AVG
RadarPLM (PA)	52.06 (+16.8)	54.87 (+5.4)	65.81 (+7.5)	57.58 (+9.9)
RadarPLM (WCE)	43.51 (+8.8)	53.95 (+4.9)	64.55 (+6.8)	54.84 (+7.7)
RadarPLM (CE)	34.73	48.96	57.80	47.16
PatchTST (PA)	47.48 (+8.1)	50.29 (+5.9)	62.42 (+7.0)	53.40 (+7.0)
PatchTST (WCE)	46.68 (+7.8)	48.96 (+5.0)	57.80 (+2.9)	51.15 (+5.2)
PatchTST (CE)	38.91	43.92	54.89	45.91

the fine-tuned PLM-based model outperforms the reference model by approximately **3%-18%** across various datasets. Notably, despite this substantial performance gap, employing the reference model to construct the preference-aware loss still leads to significant performance gains, demonstrating that our method effectively realizes a compelling weak-to-strong generalization capability.

Although the preceding results are promising, a direct comparison between the proposed preference-aware (PA) loss and the conventional end-to-end cross-entropy (CE) loss remains lacking. To bridge this gap, we evaluated multiple model variants: RadarLLM (PA) vs. RadarLLM (CE), and PatchTST (PA) vs. PatchTST (CE). Models labeled with (PA) adopt the proposed token-level reweighting strategy based on learning value, whereas those labeled with (CE) rely on standard cross-entropy loss. For further comparison, we include a sample-level reweighting baseline, denoted as WCE [15], where training weights are adjusted at the sample level.

As summarized in Table VII, the PA loss consistently yields superior performance across all datasets, especially under low SCR conditions. For example, RadarPLM (PA) achieves an average gain of **9.9%** over RadarPLM (CE), while PatchTST (PA) improves by **7.0%** over its CE-based counterpart. In particular, token-level reweighting in both PA variants outperforms WCE, highlighting the advantage of fine-grained reweighting in enhancing detection under challenging scenarios.

F. Analysis of the Effect of Hyperparameters on Experimental Results

We first investigate the impact of patch size on RadarPLM's performance. The results of the ablation study are summarized

TABLE VIII
PERFORMANCE COMPARISON OF RADARPLM UNDER DIFFERENT PATCH SIZES AND GPT2 LAYER NUMBERS.

Parameter	Configuration	Average DR (%)	Average IT (s)	Total / Training NP (M)
Patch Size	32	79.44	5.9259	69.39 / 2.46
	48	81.96	5.6561	69.39 / 2.46
	64	79.09	5.6222	69.39 / 2.46
GPT2 Layers	0 Layer	76.80	5.3484	41.04 / 2.44
	2 Layers	81.29	5.4812	55.22 / 2.45
	4 Layers	81.96	5.6561	69.39 / 2.46
	6 Layers	80.42	5.7331	83.57 / 2.46
	8 Layers	80.01	5.8655	97.74 / 2.47

Note: The results include average detection rate (DR), average inference time (IT), and total/training network parameters (NP, in millions). The best and second-best results are highlighted in **red** and **blue**, respectively.

in Table VIII. Using a patch size of 48 achieves the highest detection rate, outperforming configurations with smaller (32) and larger (64) patch sizes. These results highlight the importance of selecting an appropriate patch size to optimize the performance of RadarPLM.

We then investigated the impact of the number of GPT2 layers on RadarPLM's performance. Our ablation study on GPT2 layer configurations is presented in Table VIII. Activating four GPT2 layers achieves the highest detection rate, outperforming both shallower configurations and deeper ones. These results highlight two key observations: (1) a model with insufficient layers fails to fully leverage the parameter transfer capabilities of the PLM, while excess layers suffer from overfitting due to the task-irrelevant parameters in deeper layers. (2) Although utilizing more GPT2 layers significantly increases the scale of model parameters, the impact on inference latency is minimal. Specifically, the inference speed of GPT2 (8) remains approximately 91% that of GPT2 (0), as the inherent inference acceleration of the GPT architecture mitigates the computational overhead introduced by deeper layers.

V. CONCLUSION

We propose a fine-tuning framework RadarPLM that adapts the GPT2, an advanced open-source pre-trained language model, for marine radar target detection. To ensure lightweight and robust adaptation, we devise a novel lightweight adaptation module, preserving the general knowledge of the GPT2 model while significantly reducing training time and fine-tuning overhead. To mitigate overfitting on low-SCR radar signal, we develop a selective training strategy to selectively optimize different feature patches based on their online-evaluated learning values, effectively improving model robustness. Extensive experiments on real-world marine radar datasets demonstrate that RadarPLM consistently outperforms SOTA baselines, especially under low SCR conditions, achieving an average detection rate improvement exceeding 6% over the strongest competitors. Notably, under small-sample training conditions, RadarPLM surpasses the existing methods by nearly 20% at most, owing to the effective transfer of the universal knowledge in GPT-2 to the marine radar signal processing task.

REFERENCES

- [1] X. Chen, J. Guan, Z. Bao, and Y. He, "Detection and extraction of target with micromotion in spiky sea clutter via short-time fractional fourier transform," *IEEE Transactions on Geoscience and Remote Sensing*, vol. 52, no. 2, pp. 1002–1018, 2013.
- [2] P.-L. Shui, D.-C. Li, and S.-W. Xu, "Tri-feature-based detection of floating small targets in sea clutter," *IEEE Transactions on Aerospace and Electronic Systems*, vol. 50, no. 2, pp. 1416–1430, 2014.
- [3] S.-N. Shi and P.-L. Shui, "Sea-surface floating small target detection by one-class classifier in time-frequency feature space," *IEEE Transactions on Geoscience and Remote Sensing*, vol. 56, no. 11, pp. 6395–6411, 2018.
- [4] X. Bai, S. Xu, J. Zhu, Z. Guo, and P. Shui, "Floating small target detection in sea clutter based on multifeature angle variance," *IEEE Journal of Selected Topics in Applied Earth Observations and Remote Sensing*, vol. 16, pp. 9422–9436, 2023.
- [5] W. Zhao, M. Jin, G. Cui, and Y. Wang, "Eigenvalues-based detector design for radar small floating target detection in sea clutter," *IEEE Geoscience and Remote Sensing Letters*, vol. 19, pp. 1–5, 2021.
- [6] X. Chen, N. Su, Y. Huang, and J. Guan, "False-alarm-controllable radar detection for marine target based on multi features fusion via cnns," *IEEE Sensors Journal*, vol. 21, no. 7, pp. 9099–9111, 2021.
- [7] Q. Qu, Y.-L. Wang, W. Liu, and B. Li, "A false alarm controllable detection method based on cnn for sea-surface small targets," *IEEE Geoscience and Remote Sensing Letters*, vol. 19, pp. 1–5, 2022.
- [8] S. Xu, H. Ru, D. Li, P. Shui, and J. Xue, "Marine radar small target classification based on block-whitened time–frequency spectrogram and pre-trained cnn," *IEEE Transactions on Geoscience and Remote Sensing*, vol. 61, pp. 1–11, 2023.
- [9] S. Xia, Y. Kong, K. Xiong, and G. Cui, "Target detection in sea clutter via contrastive learning," *IEEE Transactions on Instrumentation and Measurement*, vol. 72, pp. 1–13, 2023.
- [10] H. Wan, X. Tian, J. Liang, and X. Shen, "Sequence-feature detection of small targets in sea clutter based on bi-ilstm," *IEEE Transactions on Geoscience and Remote Sensing*, vol. 60, pp. 1–11, 2022.
- [11] N. Su, X. Chen, J. Guan, and Y. Huang, "Maritime target detection based on radar graph data and graph convolutional network," *IEEE Geoscience and Remote Sensing Letters*, vol. 19, pp. 1–5, 2021.
- [12] Y. Chang, X. Wang, J. Wang, Y. Wu, L. Yang, K. Zhu, H. Chen, X. Yi, C. Wang, Y. Wang *et al.*, "A survey on evaluation of large language models," *ACM transactions on intelligent systems and technology*, vol. 15, no. 3, pp. 1–45, 2024.
- [13] T. Zhou, P. Niu, L. Sun, R. Jin *et al.*, "One fits all: Power general time series analysis by pretrained lm," *Advances in neural information processing systems*, vol. 36, pp. 43 322–43 355, 2023.
- [14] Z. Xu, T. Zheng, and L. Dai, "Llm-empowered near-field communications for low-altitude economy," *IEEE Transactions on Communications*, pp. 1–1, 2025.
- [15] S. Mindermann, J. M. Brauner, M. T. Razzak, M. Sharma, A. Kirsch, W. Xu, B. Höltingen, A. N. Gomez, A. Morisot, S. Farquhar *et al.*, "Prioritized training on points that are learnable, worth learning, and not yet learnt," in *International Conference on Machine Learning*. PMLR, 2022, pp. 15 630–15 649.
- [16] Q. Hu, L. Zhang, X. Wang, G. Li, Y. Liu, and X.-P. Zhang, "When marine radar target detection meets pretrained large language models," in

IGARSS 2025-2025 IEEE International Geoscience and Remote Sensing Symposium, 2025, in press.

- [17] Y. Wang, W. Zhao, X. Wang, J. Chen, H. Li, and G. Cui, "Nonhomogeneous sea clutter suppression using complex-valued u-net model," *IEEE Geoscience and Remote Sensing Letters*, vol. 19, pp. 1–5, 2022.
- [18] N. Su, X. Chen, J. Guan, Y. Huang, X. Wang, and Y. Xue, "Radar maritime target detection via spatial-temporal feature attention graph convolutional network," *IEEE Transactions on Geoscience and Remote Sensing*, vol. 62, pp. 1–15, 2024.
- [19] J. Wang and S. Li, "Maritime radar target detection model self-evolution based on semisupervised learning," *IEEE Transactions on Geoscience and Remote Sensing*, vol. 62, pp. 1–11, 2023.
- [20] Y. Wang, X. Chen, X. Wang, C. Zang, W. Zhao, and G. Cui, "Radar detection self-evolution based on incremental learning in time-varying clutter environments," *IEEE Transactions on Instrumentation and Measurement*, vol. 73, pp. 1–13, 2024.
- [21] A. Radford, J. Wu, R. Child, D. Luan, D. Amodei, I. Sutskever *et al.*, "Language models are unsupervised multitask learners," *OpenAI blog*, vol. 1, no. 8, p. 9, 2019.
- [22] B. Liu, X. Liu, S. Gao, X. Cheng, and L. Yang, "Llm4cp: Adapting large language models for channel prediction," *Journal of Communications and Information Networks*, vol. 9, no. 2, pp. 113–125, 2024.
- [23] Y. Sheng, K. Huang, L. Liang, P. Liu, S. Jin, and G. Y. Li, "Beam prediction based on large language models," *IEEE Wireless Communications Letters*, 2025.
- [24] T. Zheng and L. Dai, "Large language model enabled multi-task physical layer network," *IEEE Transactions on Communications*, 2025.
- [25] T. An, Y. Zhou, H. Zou, and J. Yang, "Iot-llm: A framework for enhancing large language model reasoning from real-world sensor data," *Patterns*, 2025.
- [26] M. Tan, M. Merrill, V. Gupta, T. Althoff, and T. Hartvigsen, "Are language models actually useful for time series forecasting?" *Advances in Neural Information Processing Systems*, vol. 37, pp. 60 162–60 191, 2024.
- [27] A. Vaswani, N. Shazeer, N. Parmar, J. Uszkoreit, L. Jones, A. N. Gomez, L. Kaiser, and I. Polosukhin, "Attention is all you need," *arXiv preprint arXiv:1706.03762*, 2017.
- [28] E. J. Hu, Y. Shen, P. Wallis, Z. Allen-Zhu, Y. Li, S. Wang, L. Wang, W. Chen *et al.*, "Lora: Low-rank adaptation of large language models." *ICLR*, vol. 1, no. 2, p. 3, 2022.
- [29] J.-Y. Li, X.-J. Zhang, Z.-J. Zhao, P.-L. Shui, and S.-W. Xu, "Small target classification of maritime radars using standardized time-frequency distribution images and residual networks with improved focal loss," *IEEE Transactions on Instrumentation and Measurement*, vol. 74, pp. 1–17, 2025.
- [30] Q. Qu, H. Chen, W. Liu, B. Li, and Y.-L. Wang, "Neural network based false alarm controllable detector for weak targets via a differentiable np loss," *IEEE Transactions on Aerospace and Electronic Systems*, pp. 1–13, 2025.
- [31] A. Kendall, Y. Gal, and R. Cipolla, "Multi-task learning using uncertainty to weigh losses for scene geometry and semantics," in *Proceedings of the IEEE conference on computer vision and pattern recognition*, 2018, pp. 7482–7491.
- [32] K. Cho, "Learning phrase representations using rnn encoder-decoder for statistical machine translation," *arXiv preprint arXiv:1406.1078*, 2014.
- [33] Y. Nie, N. H. Nguyen, P. Sinthong, and J. Kalagnanam, "A time series is worth 64 words: Long-term forecasting with transformers," *arXiv preprint arXiv:2211.14730*, 2022.
- [34] Q. Qu, W. Liu, J. Wang, B. Li, N. Liu, and Y.-L. Wang, "Enhanced cnn-based small target detection in sea clutter with controllable false alarm," *IEEE Sensors Journal*, vol. 23, no. 9, pp. 10 193–10 205, 2023.